

Quantitative Chemical Mapping of Nanostructured “Onionlike” Poly(methyl methacrylate)/Polystyrene Composite Particles by Soft X-ray Microscopy

R. Takekoh,^{†,‡} M. Okubo,^{†,§} T. Araki,^{†,||} H. D. H. Stöver,^{†,#} and A. P. Hitchcock^{*,†}

Graduate School of Science and Technology, Kobe University, Kobe, 657-8501, Japan, and Department of Chemistry and BIMR, McMaster University, Hamilton, ON, L8S 4M1, Canada

Received July 9, 2004; Revised Manuscript Received November 9, 2004

ABSTRACT: In earlier work, we have produced micrometer-sized, monodisperse, poly(methyl methacrylate)/polystyrene (PMMA/PS) composite particles having a multilayered structure. A challenge to developing applications for these multilayered particles is the quantitative, spatially resolved chemical analysis of their onionlike layered structure, where some layers are thinner than 100 nm. Scanning transmission X-ray microscopy (STXM) has a spatial resolution of better than 50 nm and sufficient chemical contrast to both observe and quantitate the composition of individual layers without staining. The results of quantitative chemical analysis of the particles and standard P(S-co-MMA) random copolymers by STXM are shown to be in good agreement with ¹H NMR measurements of their average composition. Results from chemical quantification of the individual layers of the onionlike particles by STXM are reported. Analyses of samples prepared with and without embedding in epoxy are compared. Our analysis takes into account the finite spatial resolution of the STXM. The extent of intermixing between layers was estimated by comparing the measured results to those generated from an assumed instrumental response function and trial compositional structures. This analysis suggests that the individual layers are relatively pure, although small amounts of intermixing (<15%) are also consistent with the results. Possible origins of intermixed layers are indicated and ways to achieve more pure layers are suggested.

1. Introduction

Polymer particles have attracted much interest in academia and industry due to their many current and potential applications throughout chemistry, life sciences, and technology. They impact many technologies, including paper coating, adhesives, immunological screening and diagnostics, and drug and vaccine delivery. Control of the morphology of polymer particles and its relation to physical and mechanical properties is of great importance for industrial performance. Therefore, many studies have focused on controlling the morphology of particles and have led to diverse morphologies including core/shell,¹ hemispherical,² sandwichlike,³ snowmanlike,⁴ and golfball-like⁵ structures.

Recently we have successfully produced micrometer-sized, monodisperse, “onionlike” multilayered poly(methyl methacrylate)/polystyrene (PMMA/PS) particles by seeded dispersion polymerization (SDP) and solvent-absorbing/releasing methods (SARM).⁶ These composite particles have potential as impact-resistant materials and as microprobes for near-field scanning optical microscopy. The formation mechanism of these particles has been discussed in detail elsewhere.^{7,8}

To optimize the multilayered structure of such composite materials for particular applications, one needs, first, to visualize the internal structure at high spatial resolution and, second, to perform quantitative chemical analysis at the spatial scale of that structure. Tradi-

tional chemical spectroscopies used for polymer studies, such as infrared and nuclear magnetic resonance (NMR), can easily differentiate chemical species but do not have the necessary submicrometer spatial resolution. Analytical transmission and scanning transmission electron microscopes ((S)TEM) have excellent spatial resolution and are very useful to visualize submicrometer structures, but electron microscopy typically does not offer sufficient chemical sensitivity for quantitative chemical mapping beyond the elemental level. Indeed, one cannot always be sure whether features observed by electron (or optical) microscopy arise from chemical inhomogeneity or simply from density or thickness variations of the specimen. Selective staining can be used to increase the chemical sensitivity, but this remains an indirect method, one which may lead to artifacts. Furthermore, high-resolution electron microscopy of polymers is experimentally difficult on account of the radiation damage caused by the high-energy electron beam.

Recently, analytical soft X-ray microscopy has been developed and applied to study polymers.^{9,10} The scanning transmission X-ray microscope (STXM)¹¹ at the Advanced Light Source (ALS) used in this work provides images with better than 50 nm spatial resolution and a photon energy resolution of about 100 meV. Near-edge X-ray absorption fine structure (NEXAFS) spectral signals¹² are the basis for the chemical speciation. By chemical speciation we mean the quantitative mapping of specific chemical compounds from fine details of the NEXAFS spectra, as opposed to elemental mapping, as can be obtained from X-ray fluorescence analysis or other techniques. Here we have used carbon 1s (C 1s) spectroscopy, but other core edges, particularly nitrogen 1s (N 1s) and oxygen 1s (O 1s), can also be very useful in applying STXM to polymers. The photon flux transmitted through a column of the sample is related to the

* Corresponding author. E-mail: aph@mcmaster.ca. Telephone: 905-525-9140 x24749. Fax: 905-521-2773.

[†] Kobe University.

[‡] E-mail: takeko@sc.sumitomo-chem.co.jp.

[§] E-mail: okubo@cx.kobe-u.ac.jp.

^{||} McMaster University.

^{||} E-mail: TAraki@lbl.gov.

[#] E-mail: stoverh@mcmaster.ca.

Table 1. Preparation of PMMA/PS/Toluene (1/1/20, Weight Ratio) Particles by Combining the PMMA/PS Composite Particle Emulsion and a Toluene Emulsion Prepared with an Ultrasonic Homogenizer

ingredient	mass (g)
(A) PMMA/PS Emulsion	
PMMA/PS particles	0.1
methanol	3.3
water	6.6
(B) Toluene Emulsion	
toluene	10
SDS	0.01
methanol	6.7
water	3.3

^a Abbreviations: PMMA, poly(methyl methacrylate); PS, polystyrene; SDS, sodium dodecyl sulfate.

amount of each compound present, with a weighting given by the mass absorption coefficient of that compound at the photon energy employed. Since NEXAFS spectra for pure materials can be converted easily to accurate mass or linear absorption scales, STXM can be used for quantification at submicrometer scales.^{10,11} While radiation damage is still a concern, for equivalent spatially resolved analysis, it has been shown to be about 2 orders of magnitude lower in STXM than in analytical electron microscopy.¹³

Previously¹⁴ we used STXM to study core/shell microspheres consisting of 2 μm polydivinylbenzene (DVB55) cores coated with 400–900 nm wide shells composed of poly(DVB55-*co*-EDMA), a random copolymer of DVB55 and ethylene dimethacrylate (EDMA). The chemical composition, core/shell morphology, and porosity of these structured microspheres have been investigated quantitatively.¹⁴ In this paper, micrometer-sized, monodisperse, multilayered PMMA/PS particles with layer dimensions of ~ 100 nm are measured quantitatively with STXM. This research not only produced detailed quantitative chemical maps of PMMA/PS composite particles, but also evaluated the accuracy of the quantitative analysis by comparison of STXM and ¹H NMR of samples of a series of P(St-*co*-MMA) copolymers and investigated the impact of various sample preparation methods on the analysis. Together these results show that STXM can provide reliable chemical speciation at sub-100 nm spatial resolution of materials consisting of combinations of PMMA and PS, which are common industrial polymers.

2. Experimental Section

2.1. Sample Preparation. Methyl methacrylate (MMA) and styrene were purified by distillation under reduced pressure in a nitrogen atmosphere. Reagent grade 2,2'-azobis(isobutyronitrile) (AIBN) was purified by recrystallization. All other materials were used without further purification including guaranteed reagent grade methanol, toluene, and sodium dodecyl sulfate (SDS).

Micrometer sized, monodisperse, multilayered PMMA/PS composite particles were prepared by seeded dispersion polymerization and solvent-absorbing/releasing methods as described previously.⁶ First, monodisperse PMMA seed particles were produced by dispersion polymerization. Second, seeded dispersion polymerizations of styrene were carried out in the presence of the PMMA seed particles. Swelling of the resulting PMMA/PS composite particles with toluene was carried out under the conditions listed in Table 1. Toluene was emulsified in a methanol/water mixture (1/2, w/w) containing 0.1% SDS with an ultrasonic homogenizer at 0 $^{\circ}\text{C}$ for 10 min. The toluene emulsion was combined with the particle composite emulsion and stirred with a magnetic stirrer at 140 rpm for 2 h at room

Table 2. Formulations and STXM and NMR Analysis of P(St-*co*-MMA) Standard Samples Prepared by Solution Polymerizations at 60 $^{\circ}\text{C}$ for 3 h^a

target (% PS)	ingredient				NMR-PS ^b $\pm 3\%$	STXM-PS ^c $\pm 4\%$
	St (g)	MMA (g)	AIBN (g)	toluene (g)		
0	0	5.0	0.05	10	(0)	-3
25	1.25	3.75	0.05	10	35	32
50	2.50	2.50	0.05	10	48	52
75	3.75	1.25	0.05	10	72	68
100	5.0	0	0.05	10	(100)	98

^a Abbreviations: St, styrene; MMA, methyl methacrylate; AIBN, 2,2'-azobis(isobutyronitrile). ^b The spectra of the pure materials were used as references and were assumed to be pure. ^c The spectra of different samples of the pure materials were analyzed by the same quantitative fitting procedure to check for precision.

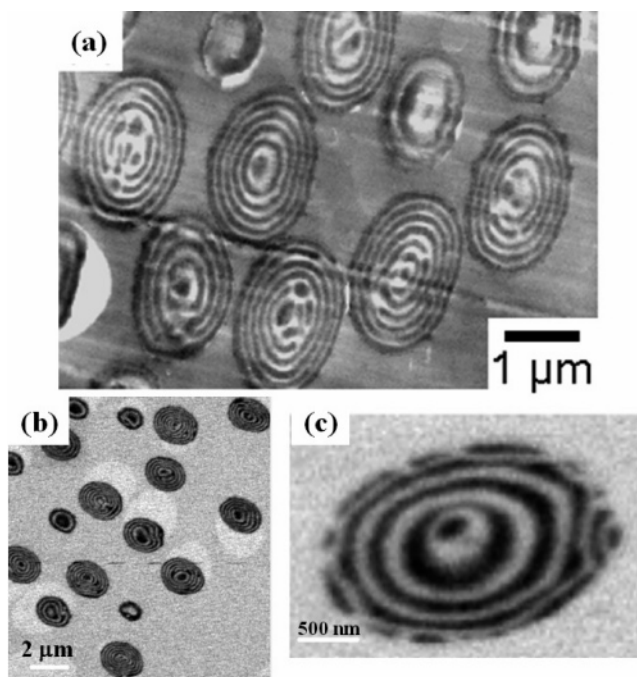


Figure 1. (a) TEM image of onion particles stained with RuO_4 . (b) STXM image at 285.1 eV (only PS is strongly absorbing) of a group of particles embedded in epoxy resin. (c) STXM image of a cryo microtomed sample recorded at 285.1 eV. Note that the two STXM images are as-recorded, transmission data in which the PS-rich regions appear dark.

temperature to prepare toluene-swollen particles. Toluene was then allowed to evaporate naturally at room temperature from 24.5 mL of the emulsion placed in an uncovered glass cylindrical vessel whose evaporation areas between the emulsion and air was 10 cm^2 .

Two types of microtomed thin sections of multilayered composite particles were prepared. In the first procedure, the particles were embedded in a new epoxy resin (trimethylol propane triglycidyl ether and 4,4'-methylenebis(2-methylcyclohexylamine)) optimized for STXM applications,¹⁵ cured, and ultramicrotomed to form sections between 50 and 100 nm thick. (*Caution!* Like many epoxides, these chemicals are known carcinogens. The epoxy preparation and embedding must be carried out in a fume hood with appropriate precautions.) This epoxy resin does not contain aromatic or carbonyl groups and thus provides minimal interference with quantification of PS and PMMA by NEXAFS. Curing is carried out at elevated temperature (60 $^{\circ}\text{C}$) for several days, until a suitable toughness for microtoming is reached, but stopped before the resin becomes too brittle. As during embedding the low molecular weight components of the resin may be able to diffuse into or slightly swell the multilayered particles, some

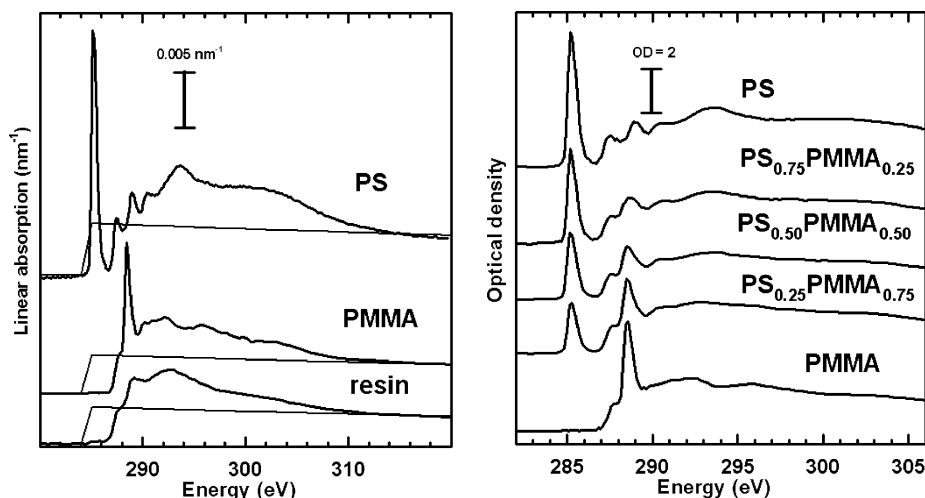


Figure 2. (a) Spectra of resin, PS, PMMA and block copolymers of variable composition, converted to a linear absorption scale. The thin curves are the elemental response for 1 nm thickness of the pure material at standard density. Offsets are used for clarity. (b) C 1s spectra of pure PS, pure-PMMA, and three P(S-*co*-MMA) random copolymers (block copolymers were used to ensure homogeneity at the spatial scale sampled). This set of samples was used to check the quantitative capabilities of STXM.

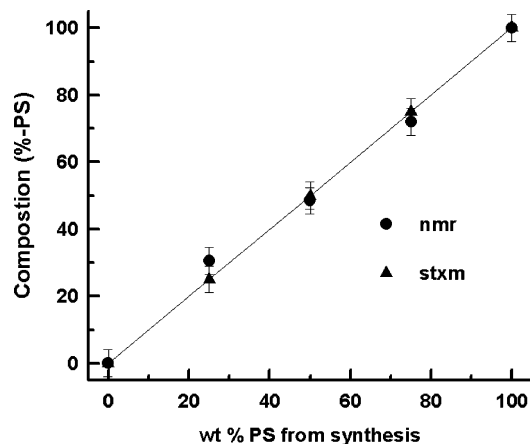


Figure 3. Plot of the PS composition (vol-%) of a series of P(S-*co*-MMA) random copolymers derived from STXM and ¹H NMR. The x-axis is the expected composition based on the synthesis.

microspheres were additionally cryoultramicrotomed in absence of resin. A sample dispersed in methanol was frozen at -120 °C and cryomicrotomed to approximately 100 nm thickness. While frozen, the microtomed section was laid flat on a Si wafer containing a 100 nm thick Si₃N₄ window with an area of 750 μm × 750 μm.

P(S-*co*-MMA) random copolymers, used as standards to calibrate the STXM response, were prepared by solution polymerization using the formulations listed in Table 2. After purification by reprecipitation, thin films of these copolymers were cast from toluene (0.025 wt % solution) onto Si₃N₄ membrane windows.

2.2. Characterization of Multilayered Microspheres.

TEM images of the resulting microtome sections revealed the expected multilayered structure.⁶ Figure 1a shows an example of a TEM image of monodisperse multilayered microspheres prepared by this method. The overall multilayered morphology is clearly visible in TEM because the sample was stained by RuO₄, which bonds mainly to PS and thus gives higher electron density and contrast to regions rich in PS.

2.3. Scanning Transmission X-ray Microscopy (STXM) Measurements. C 1s images were recorded with the polymer STXM¹¹ at beamline 5.3.2¹⁶ of the Advanced Light Source (ALS). Parts b and c of Figure 1 are sample STXM images recorded at 285.1 eV, the energy of the intense C 1s → π*_{C=C} transition in PS. The imaging is performed in 1/3 atm of helium. The transmitted photon flux is measured with single photon

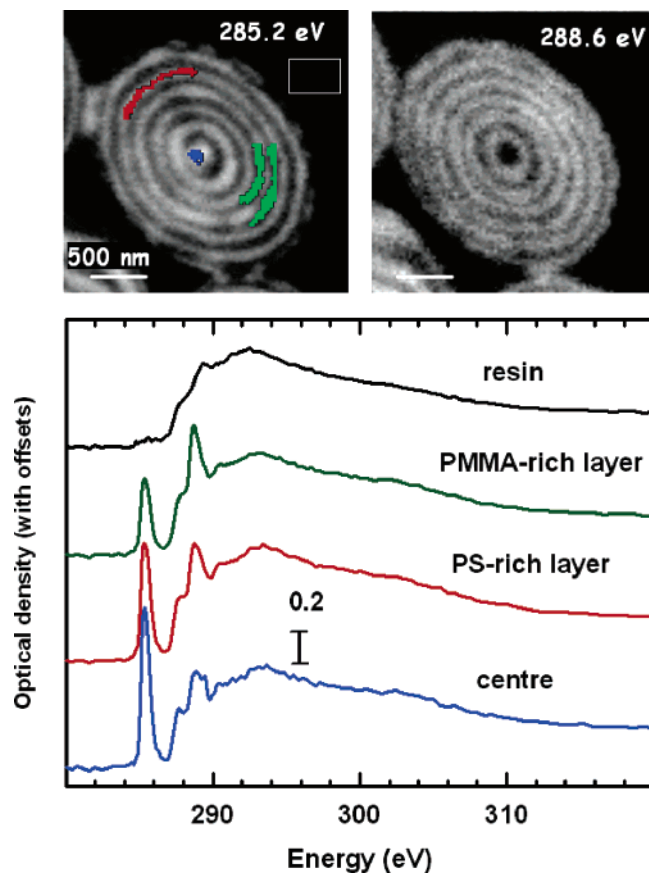


Figure 4. (Upper) Optical density images at 285.1 (PS-bright) and 288.6 eV (PMMA-bright) of an onion particle. (Lower) Spectra of the indicated regions of this onion particle, as acquired by an image sequence.

counting using a phosphor converter (P43, GdO₂S₂:Tb) and a high-performance photomultiplier tube (Hamamatsu 647P). This detection system is linear up to ~30 MHz when using a divide-by-10 amplifier to avoid nonlinearity in the pulse processing. Typical incident flux is ~5 × 10⁶ photons/s at 300 eV, with the ALS storage ring running at 1.9 GeV and 400 mA and with monochromator entrance and exit slits set to provide 100 meV fwhm energy resolution in the carbon 1s region ($E/\Delta E \sim 3000$). Typically, counting periods (dwell times) of 1 ms per pixel were used for imaging and quantitative analysis. The spatial resolution of the microscope is better than

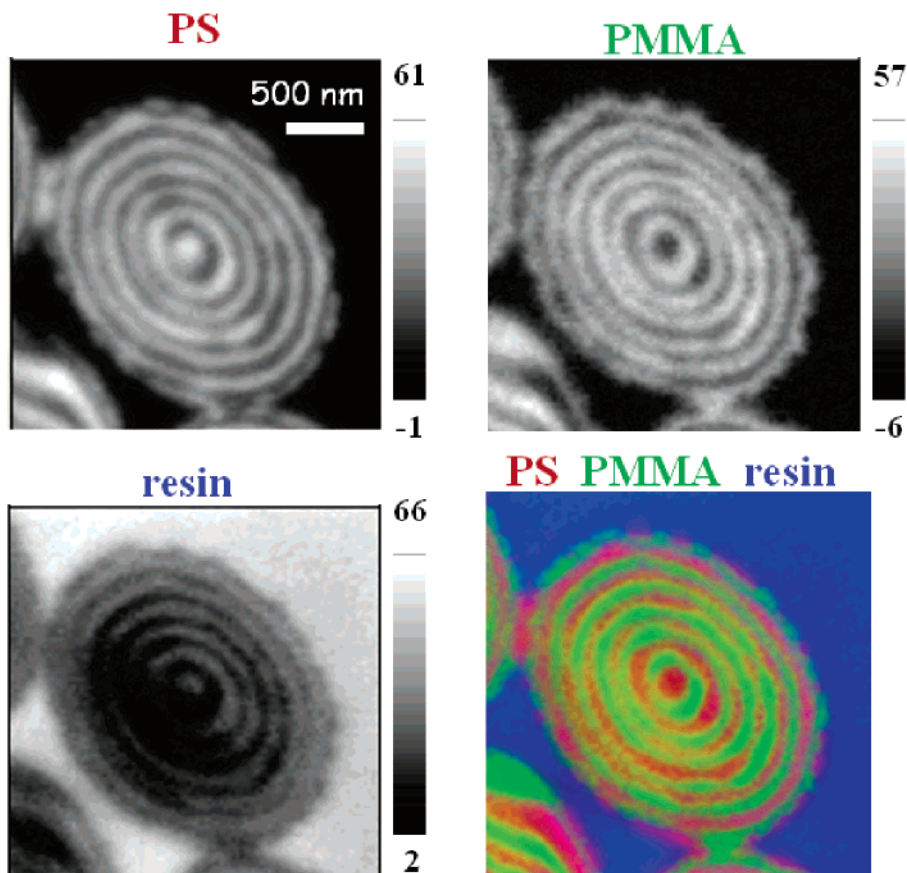


Figure 5. PS, PMMA, and resin component maps derived from fitting 121 images in the C 1s regime of the resin-embedded PMMA/PS particle in Figure 4 with the linear absorption reference spectra plotted in Figure 2a. The gray scales are quantitative thickness in nanometers. A color coded composite map, in which the three components are independently scaled, is also included.

50 nm, limited by the characteristics of the focusing Fresnel zone plate (at the time of these measurements the zone plate used was 155 μm diameter, with 35 nm outer zone width, giving a spatial resolution at the diffraction limit of 42 nm). While microscope characterization was not performed at exactly the same time as the measurements were performed, tests of the spatial resolution as a function of the exit slit parameters carried out in the months prior to, and after the analysis indicated that when the STXM is operated with the (30 \times 30 μm) exit slits that were used for these measurements, the diffraction limited resolution of the zone plate is achieved, as determined by careful evaluation of images recorded from high contrast electron beam lithography test patterns.

Images and image sequences were recorded at selected energies through the C 1s region (280–320 eV). The methodology and first generation analysis software for image sequence (“stack”) acquisition and analysis were developed by Chris Jacobsen.¹⁷ The analysis of these data was performed using enhanced image sequence analysis routines in aXis2000.¹⁸ After each image sequence measurement, an image was recorded at a photon energy sensitive to radiation damage (288.6 eV, the energy of the C 1s $\rightarrow \pi^*_{\text{C=O}}$ transition in PMMA) in order to characterize the extent of radiation damage. When full spectral image sequences consisting of 121 energies are used, significant damage occurs. However, high quality analytical results could be achieved using singular value decomposition (SVD) analysis¹⁹ of a reduced set of 12 images at energies carefully chosen to differentiate the three chemical species of this system. For these so-called “short stacks” negligible radiation damage occurred. In other studies the dose–damage response for STXM of pure PMMA has been characterized,^{20,21} and the observed damage rates to the PMMA component of the onion particles are consistent with these results. C 1s spectra of the pure polymeric components (PS, PMMA and epoxy resin) were recorded with the same instrument, converted to absolute mass absorption, and used as

reference spectra for quantitation. P(S-co-MMA) films prepared by solution casting of random copolymers were measured by STXM as standard samples for quantification. The photon energy scale was calibrated by recording the spectrum of the C 1s $\rightarrow 3s/3p$ Rydberg states of CO₂ in the STXM. This calibration places the maximum of the strong $\pi^*_{\text{C=C}}$ of PS to 285.15 eV.²² The incident flux was measured quasi-simultaneously with each series of images by measuring the signal through an adjacent empty grid cell. This was used to convert the transmission images to optical density.

3. Results and Discussion

3.1. Calibration of P(S-co-MMA) Quantitation.

Figure 2a presents the C 1s spectra of pure PS, PMMA, and the epoxy resin, on a linear absorption scale (optical density per nm thickness at standard density). The intensity scales, which provide quantitation when used as reference spectra in fits, are set by matching the signal outside the structured near edge regions to the elemental response for 1 nm of normal density material ($d_{\text{PS}} = 1.05 \text{ g/cm}^3$, $d_{\text{PMMA}} = 1.18 \text{ g/cm}^3$, $d_{\text{resin}} = 1.0 \text{ g/cm}^3$) which is indicated for each species in Figure 2a (Note: the intensity is scaled to that for 1 nm, so that when these spectra are used as reference standards, the resulting fit coefficients give the equivalent thickness of pure material directly in nanometers). The accuracy of the quantitative analysis by NEXAFS in STXM was checked by recording the C 1s spectra of neat PS, PMMA and of three P(S-co-MMA) copolymer standards, using a defocused beam to reduce radiation damage. Figure 2b presents these spectra. Figure 3 plots the composition measured by ¹H NMR and STXM, against the theoretical composition expected from the comonomer feed

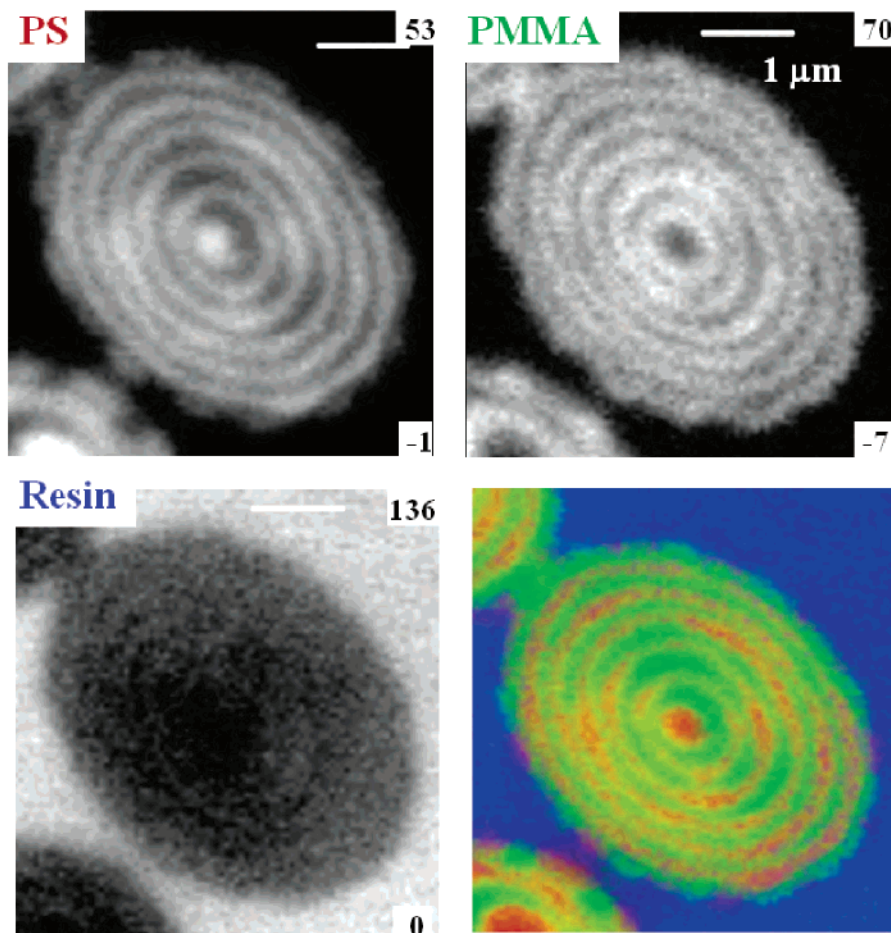


Figure 6. PS, PMMA and resin component maps derived from fitting 12 images in the C 1s regime of a resin-embedded PMMA/PS particle with the linear absorption reference spectra plotted in Figure 2a. A color coded composite map, in which the three components are independently scaled, is also included. The numbers in the lower and upper right corners of the composite maps are the lower and upper gray scale limits in nanometers of that component.

ratios. The STXM result was determined by fitting the spectra of the three copolymer samples to the reference spectra of neat PS and PMMA. The fitting coefficients give an absolute quantitation, since the reference spectra are on quantitative linear absorption coefficient scales. The ^1H NMR based composition was determined from peak integration, and linear scaling to the response of the pure materials. For the same samples, the STXM and ^1H NMR values (summarized in Table 2) agree within mutual error bars and are quite close to the theoretical composition expected from the feed ratios. Small deviations of the observed from the theoretical composition are likely due to the slight tendency of styrene and MMA to form alternating copolymers, which would increase the incorporation of the minor comonomer (i.e., styrene for 25% styrene copolymer) in the case of nonquantitative conversion to polymer.

3.2. STXM Measurements of PMMA/PS “Onion”-like Particles. The STXM images (Figure 1, parts b and c) clearly show the sub-100 nm scale, multilayered structure of the PMMA/PS composite particles with almost the same quality as the TEM image (Figure 1a). Parts a and b of Figure 4 are STXM images on an optical density scale at 285.1 eV (PS absorbing) and 288.6 eV (PMMA more absorbing than PS) of near-equatorial cross sections of PMMA/PS onionlike particles embedded in epoxy resin. The dramatic inversion of contrast between these two energies clearly illustrates the chemical sensitivity and compositional information

provided by the STXM technique. Figure 4c compares the spectra of the center of the particle, two of the outer rings of opposite contrast, and the embedding resin. The regions of the sample from which the spectra were extracted are indicated in Figure 4a. The center of the microsphere shows a spectrum which is very similar to PS. This shows that the initial multilayered structure was dissolved by the toluene and completely reconstructed from PMMA-core/PS-shell composite particles by the SARM mechanism as discussed elsewhere.⁸ The outer rings of the microsphere show spectra which display features of both PMMA and PS, with variable composition. Finally the spectrum of the embedding resin is that of the pure resin, with no absorption due to styrene or MMA. These results indicate that STXM has both the spatial resolution and chemical contrast to distinguish PS, PMMA and resin on a sub-100 nm scale.

Figure 5 shows results of a chemical analysis of a C 1s image sequence, in the form of quantitative chemical maps of the PS, PMMA and resin components of the particle whose images and regional spectra are displayed in Figure 4. These maps are derived by fitting the C 1s image sequence (121 images from 280 to 320 eV) to the spectra of the pure materials. The gray scale limits indicate the equivalent thickness in nm of pure PS, PMMA or resin. In addition to the individual component maps, a color coded composite (red = PS, green = PMMA, blue = resin) is included to display the

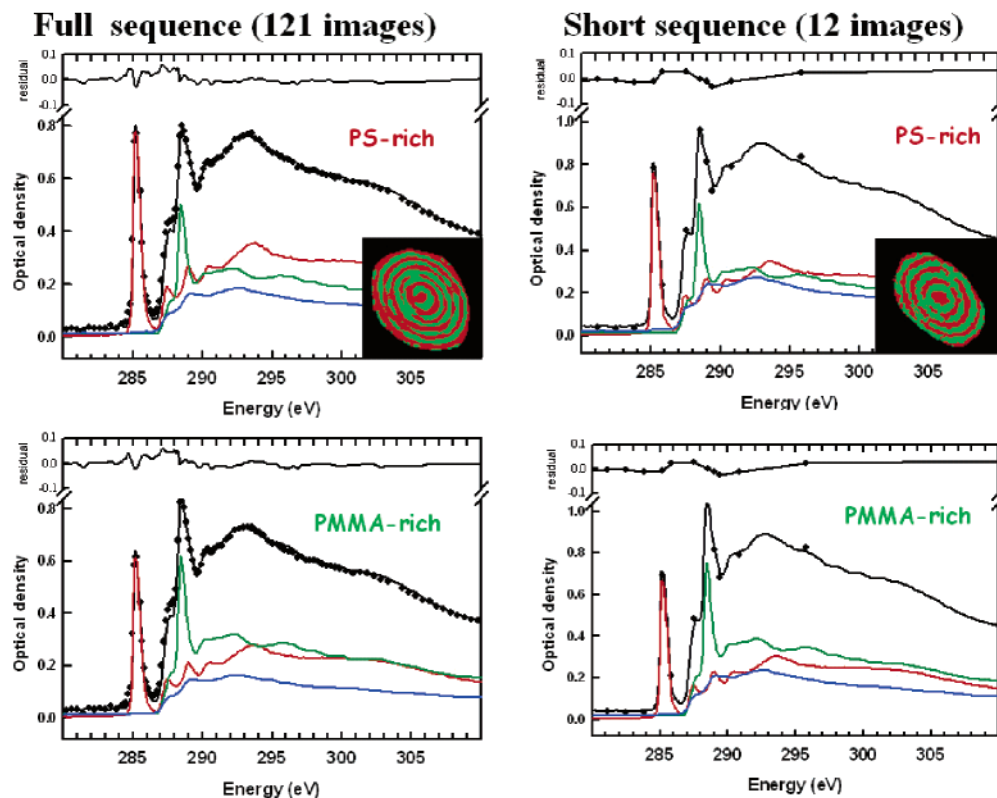


Figure 7. Quantitative curve fits for PS-rich, PMMA-rich, and the total particle signal for the 121 image sequence (left) and the 12 image sequence (right). The insert figures indicate the spatial regions from which the spectra were selected (red = PS-rich, green = PMMA-rich).

Table 3. Compositions of Particles (Equivalent Nanometer Thickness) Determined by STXM by Image Sequence Analysis of PMMA/PS Particles

A. Resin-Embedded PMMA/PS Particles

region	full image sequence (121 energies)					short image sequence (12 energies)				
	PS	PMMA ^a	resin	sum	PS/PMMA	PS	PMMA	resin	sum	PS/PMMA
PS-rich	35	36	25	96	0.97	33	44	37	114	0.75
PMMA-rich	27	44	22	93	0.61	29	53	32	114	0.55
all	31	40	21	92	0.78	31	49	34	114	0.63

B. Cryomicrotomed

region	particle #1				particle #2			
	PS	PMMA	sum	PS/PMMA	PS	PMMA	sum	PS/PMMA
PS-rich	28.5	30.0	58.5	0.95	32	29	61	1.10
PMMA-rich	15	39	54	0.38	13	43	56	0.30
all	20	35	55	0.57	22	34	56	0.64

^a The amount of PMMA is very likely underestimated in the full image sequence measurement due to radiation damage.

spatial relationships of the components. This quantitative analysis suggests that each layer is a mixture of PS and PMMA, with only the composition being modulated between the layers (however, see below for a more careful interpretation of these fitting results). The resin map resulting from the fit to this image sequence indicates there is resin inside the particle. This is likely due to the uncured resin selectively swelling the PMMA/PS composite particles. The amount of resin signal decreases roughly linearly from the outside to the interior of the particle, in agreement with diffusion-limited in-penetration. The resin signal is modulated at the same periodicity as the PS and PMMA signals but the peaks in the resin are located at the boundaries of the PS-rich and PMMA-rich layers, suggesting greater ability to dissolve/penetrate in these mixed boundary regions. The resin contains nitrogen. Analysis of images,

Table 4. Analysis of C 1s Spectra Extracted from Cryo-Cut Particles at Various Thresholds, Corresponding to Positions Across PS-Rich Domains

PS range (nm)	approximate position (nm) ^a	PS (nm)	PMMA (nm)
20–25	25	22	30
25–30	50	27	31
30–35	70	32	28
35–40	80	37	28
40–45	90	42	24
>45	100	47	22

^a This is the approximate position based on an average 200 nm wide domain. The section of a PS domain plotted in Figure 11b,c is about two times larger and was chosen to allow confirmation of the (apparent) compositional gradient on the basis of a single domain. Checks at similar relative positions confirm the compositional trend found by scanning the threshold level over the whole particle.

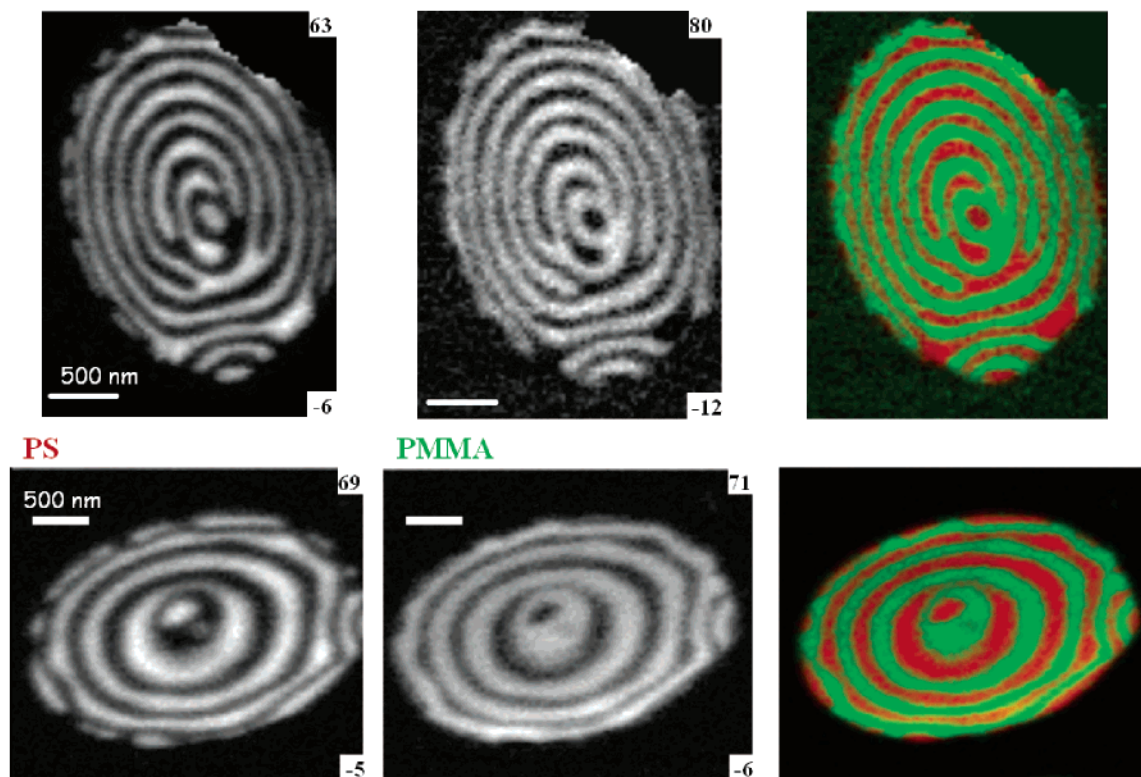


Figure 8. Quantitative PS and PMMA component maps and color composites of two particles, for which sections were prepared without embedding in the resin, but rather by freezing in an ethanol solution and cryomicrotoming. The numbers in the lower and upper right corners of the composite maps are the lower and upper gray scale limits in nm of that component. The yellow box indicates the region expanded in Figure 11.

spectra, and image sequences recorded at the N 1s edge (results not shown) gave a spatial distribution of resin in the particles very similar to that derived from the C 1s image sequence analysis, thus confirming penetration of the resin into the particle. These chemical mapping results strongly differentiate STXM from TEM in that both visual and quantitative chemical information is provided by STXM at the same time. In addition, no staining is required for STXM.

A major concern in any analytical measurement using ionizing radiation is radiation damage, and this is particularly the case when the sample contains a radiation sensitive polymer like PMMA.^{20,21} To test to what extent the damage would affect our quantitative analysis, a short image sequence consisting of images at only 12 energies was recorded from a fresh particle of the same sample. An image of the same region recorded after this measurement showed negligible damage. The chemical morphology determined from analysis of the short, low damage sequence (Figure 6) is very similar to that deduced from the full spectral image sequence. In particular the results shown in Figure 6 support the same conclusions that (i) the core is PS-rich, (ii) that the alternating onion rings have spectra which display both PS and PMMA related peaks, and (iii) that there is some resin present inside the particle. For each measurement, the average compositions of the particle, PS-rich and PMMA-rich rings was derived by using threshold masking of the component maps to define regions of interest (ROI) and then performing a curve fit to the spectra extracted from these regions. Curve fits to the PS-rich and PMMA-rich regions from both the full and short image sequence measurements are displayed in Figure 7; numerical results are summarized in Table 3. The relative amount

of PMMA deduced from analysis of the short image sequence is significantly higher, consistent with partial damage to the PMMA in the longer sequence. In addition the amount of resin present is larger in the short sequence. Since we know the resin does not exhibit damage with the doses used in the long sequence we conclude this difference is simply due to a greater degree of penetration in the particle selected for the short sequence measurement.

Quantitative results for short image sequence measurements performed on three other particles prepared by resin embedding are in agreement with those from the two particles documented in Figures 4–7 and Table 3. The central region is almost pure PS, the spectra of the alternating PS-rich and PMMA-rich differ substantially but show features of both species, and there is a significant, graded penetration of the epoxy resin into the particles.

Overall, averaging over the three resin embedded particles studied using the short image sequence, the values determined from spectra integrated over the whole particle are 33(2), 41(2), and 25(4) for the thickness in nm of the PS, PMMA, and resin respectively (note that the density and molecular weight of PS and PMMA are such that compositions expressed in mole, weight, or volume percent are all very similar²¹). The PS/PMMA ratio of 0.78(6) obtained by STXM is consistent with that of 0.84(9) obtained by ¹H NMR. These results indicate the actual overall composition of the particles is somewhat PMMA-rich relative to the theoretical 50:50 composition. This was expected as the conversion of styrene was not complete, and because some polystyrene was consumed to form small secondary particles during the seeded dispersion polymeriza-

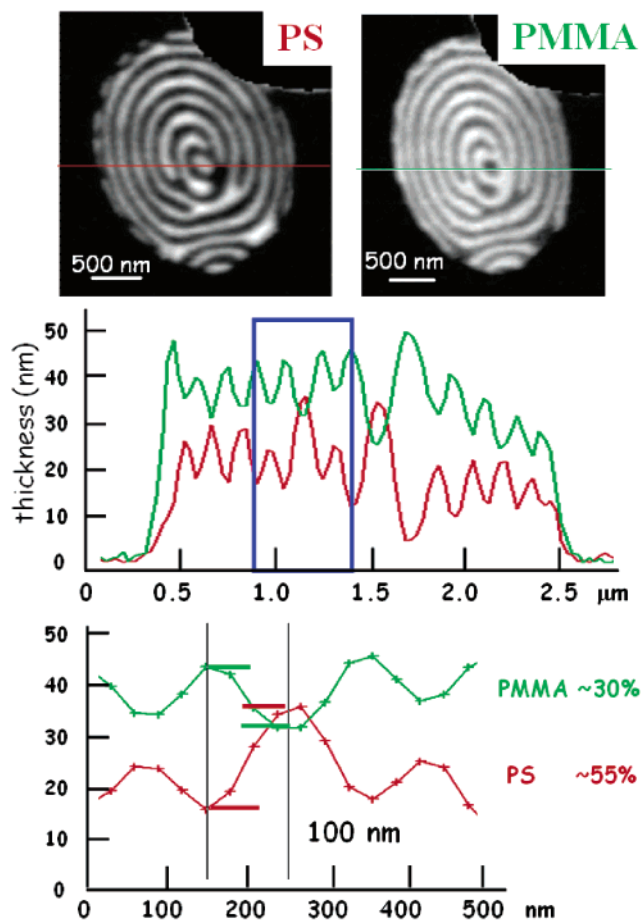


Figure 9. Intensity profiles across the center of the component maps for PS and PMMA derived for a cryo-cut particle. The expanded plot indicates the rounding at the boundary is on the order of 60 nm based on a 20–80 intensity change.

tion of styrene, which were then removed by centrifugation.

The PMMA/PS composite particles embedded in epoxy resin contain significant amounts of resin inside the particles. It is very important for polymer researchers to note this result, revealed here by STXM for the first time, as the hypothesized swelling by resin could complicate or invalidate quantitative measurements. It is possible that allowing the epoxy to partially cure prior to mixing with the particles would reduce the resin penetration phenomena. Alternatively, an aqueous-based embedding resin such as Nanoplast may be used to reduce or eliminate resin penetration. This result illustrates that STXM can provide information beyond the chemical mapping of expected components, and thus will be a very useful tool to help optimize polymer materials and sample preparation methodologies for specific applications.

To further investigate the influence of resin penetration on the compositional analysis we also examined samples prepared without resin embedding, but rather using cryo microtomy of a frozen ethanol suspension of the particles. While this sample preparation technique is more challenging, it does provide analysis without the complication of the penetrating resin. Figure 8 presents component maps and color coded composite maps for two PMMA/PS onion-type particles prepared by cryo microtomy. In the color composite maps the onion rings appear to represent purer, more-phase separated PS and PMMA, although in part that is the result of the

absence of resin signal which is present in the resin-embedded particles (Figures 5 and 6). Table 3b presents the compositional results derived from analysis of C 1s image sequences recorded from two of these cryo-microtomed particles. The quantitative results bear out the impression from the component maps and color composite presented in Figure 8. In particular, the PS-rich and PMMA-rich domains are significantly richer in the majority species than found for the resin-embedded samples, although analysis of spectra for the alternating rings (Table 3) indicates each type of ring is a mixture (however, see the following analysis). The PS/PMMA ratio in the two types of rings are slightly different in the cryo-cut samples relative to those found for the resin embedded particles.

Taken without further interpretation, the present STXM results suggest that the multilayered, PMMA/PS composite particles consist of alternating layers of mixed PMMA/PS with variable composition rather than the pure PS layers and pure PMMA layers which had been hypothesized in earlier discussions of their structure.⁸ However we note that the lateral size of the layers is only about twice that of the spatial resolution, which in itself represents the width for changing from 20 to 80% of the signal across a completely sharp interface with infinite contrast. This means there is significant signal from any given point stretching out to about 80 nm to each side. The signal in these wings of the response function leads to mixing of the signal and thus chemical information from adjacent layers. To evaluate the extent to which this might influence the present results, we have constructed model data sets consisting of alternating rings of either pure or mixed compositions, spaced as in the real onionlike particles. Figure 9 plots expanded profiles across the interfaces in the PS and PMMA component maps of one of the cryo-cut particles. These profiles were used to select parameters for multipoint smoothing of the model data sets in order to generate a rounding of the interface with a 20–80% change of about 60 nm, which is similar to that found experimentally. Figure 10 presents results from analysis of the model image sequences using exactly the same reference spectra and procedures used in analyzing the experimental data. The left panel of Figure 10 presents results for sharp interfaces with either alternating pure PS and pure PMMA layers or alternating mixed layers (one layer is 50:50, and the other layer is 25:75 in composition, which is approximately that found experimentally for the cryo-cut particles—see Table 3). Here, for each case, the analysis process gives back the same composition as was input to generate the simulated data. The right-hand part of Figure 10 presents the result of modeling with spatial resolution degradation effected by a 17-point 2-dimensional 3-point smooth. After the spatial resolution degradation, for the pure-PS/pure-PMMA system (upper part) the apparent chemical mixing is on the order of 25%. Note that this is based on analysis of only the central approximately two-thirds of the rings, to minimize the intermixing. In contrast, when the spatial degradation is applied to the system with alternating layers of mixed composition, the additional chemical mixing is only on the order of 7%. This is because each layer is already mixed chemically, so that further “apparent mixing” via finite spatial resolution has a minimal effect.

Another way to evaluate the effect of finite spatial resolution on the chemical analysis is to investigate how

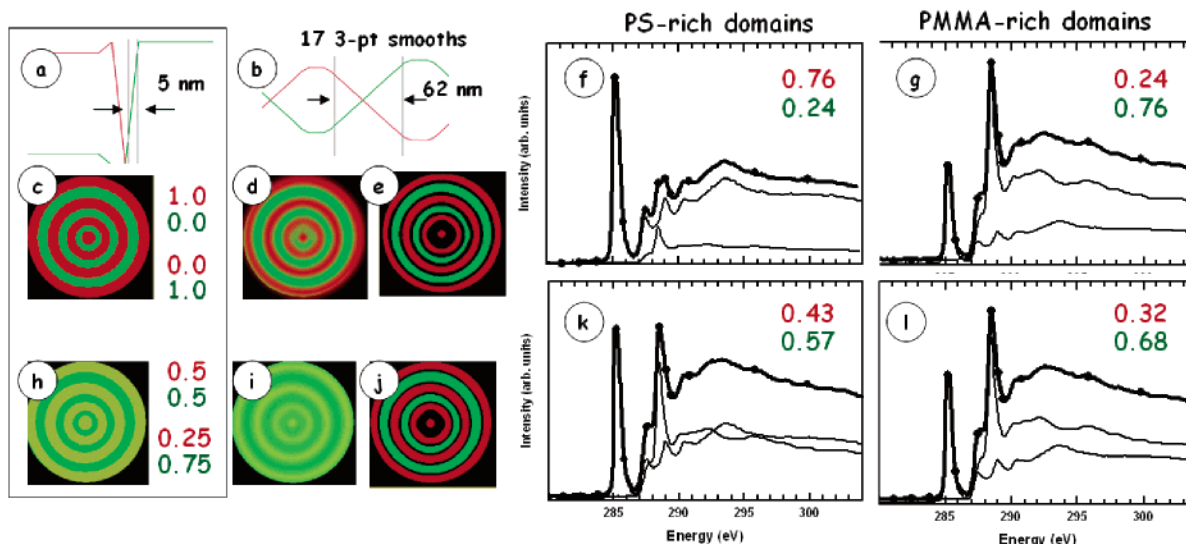


Figure 10. (a) Interface profile for a sharp interface. (b) Interface profile broadened to 62 nm by 17-point smoothing. (c) Color composite map (R=PS, G = PMMA) for pure PS, pure PMMA layers, and a sharp interface (d) color composite map for pure PS, pure PMMA layers and a broad interface. (e) Areas selected to extract PS-rich and PMMA-rich spectra from part d. (f) Fit to PS spectrum from part d. (g) Fit to PMMA spectrum from part d. (h) Color composite map for mixed PS (0.5/0.5), and mixed PMMA (0.25/0.75) layers and a sharp interface (i) color composite map for mixed PS (0.5/0.5), and mixed PMMA (0.25/0.75) layers and a broad interface. (j) areas selected to extract PS-rich and PMMA-rich spectra from part i. (k) fit to PS spectrum from part i. (l) Fit to PMMA spectrum from part i.

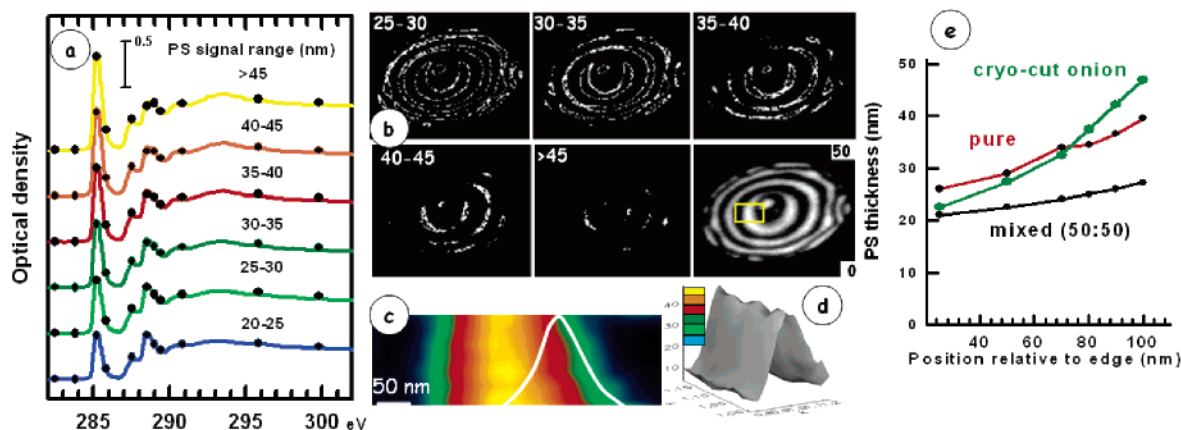


Figure 11. (a) (Circles) Extracted spectra across the PS-rich domains of a cryo-cut particle. The spectra are the average of pixels identified by the indicated range of threshold levels of the PS component map. (Lines) Fits to these extracted spectra—see Table 4 for the derived PS and PMMA content. (b) Location of pixels in the threshold ranges. (c) Expanded PS component map plot of part of one PS-rich domain of a cryo-cut particle. The indicated parts of the PS-rich domain have spectra very similar to the spectra in Figure 11a. (d) 3-d presentation of part c. (e) Comparison of the variation of PS-content across a PS-rich domain in a cryo-cut onion particle with the corresponding spatial variation found in model data sets (Figure 10) generated from pure-PS, pure-PM layers, or a 50:50 mixed layer.

the apparent composition changes across the individual domains. The modeling results for finite spatial resolution presented in Figure 10 suggest that, if the rings are pure PS and pure PMMA, a larger change in composition across the individual domains would be found, relative to the situation if the domains were intrinsically highly mixed. Figure 11 shows how the spectrum extracted from the PS-rich domains changes across the domain. Spectra were extracted from different spatial regions defined by systematic variation of a lower and upper threshold level. These spectra (circles) and their fits (lines) are presented in Figure 11a while Figure 11b indicates the corresponding spatial regions. Parts c and d of Figure 11 are images of an expanded part on one domain of the PS component map which indicates the typical spatial locations associated with the set of spectra plotted in Figure 11a. Figure 11e plots the change in the average PS contribution across the

PS-rich domains in comparison to that predicted from a similar treatment of the spatially broadened model results for pure domains and for a 50:50 mixed domain. This comparison shows that the variation in the cryo-cut onion PS-domains is more similar to that from the modeling for the pure layers, rather than that seen in the modeling of the mixed layers. From this and other modeling exercises, we tentatively conclude that the layers are most likely nearly pure PS and pure PMMA. However, because of uncertainties in the microscope response function and the exact extent of spatial blurring, intermixing at the 10–15% level cannot be ruled out.

Prior to this study, TEM observations suggested that the multilayered composite particles were fully phase-separated.⁸ However, in the toluene-swollen multilayered particles which are the precursor to these multilayered “onionlike” particles, both PMMA and PS phases

contain significant amounts of the other polymer under the conditions of SARM. Depending on the kinetics of the phase segregation, this may lead to multilayered particles in which the individual layers are mixtures rather than pure PS and pure PMMA. A surfactant is used in the process and that may be preventing full phase separation, at least for the outermost layer. We hypothesize that alternating layers with greater compositional differentiation might be produced if the evaporation time of toluene was extended by carrying out the process with a different surfactant, using a solvent mixture, or at a different temperature. While a lower evaporation temperature would increase the driving force for phase separation, a higher temperature would allow the phase separation to continue to lower compatibilizer (toluene) levels, before the increasing glass temperature freezes further diffusion. In potential optical applications for these materials a high degree of control of the compositional variation of the layers is required in order to achieve desired refractive index variations. Further development of the SARM conditions, assisted by STXM analysis, may achieve suitable materials.

Summary

STXM has been used to provide images and spatially resolved quantitative compositional information on multicomponent PMMA/PS "onionlike" polymers with a spatial resolution better than 50 nm. The images obtained by STXM had similar quality to those obtained by TEM of stained samples. Quantitative analysis of the NEXAFS spectra of reference polymers and the average spectrum of the "onionlike" particles obtained by STXM was shown to provide composition results equal to those obtained by ^1H NMR. Initial examination of the spatially resolved quantitative analysis indicated that the alternating layers of the "onionlike" structure consisted of a compositional modulation rather than pure PMMA and PS layers. However when the limited spatial resolution of STXM was taken into account, the data suggests the layers are in fact relatively pure, although some mixing is also consistent with the results. Possible origins of intermixed layers are indicated and ways to achieve more pure layers are suggested.

Determining the chemical basis for 100 nm scale ordered structures within 2- μm -sized, monodisperse, multilayered samples is a very good example of the polymer analysis capabilities of STXM. Quantitative chemical mapping of polymers by STXM is a very useful method which is likely to become indispensable to state-of-the-art polymer chemistry. The development of nanoscale synthetic techniques must be accompanied by corresponding nanoscale analytical tools, such as STXM analysis. In combination they will accelerate the application of "onionlike" multilayered particles for optical materials, as spacers for liquid crystal display applications, probes for near-field scanning optical microscopes, and photonic crystals.

Acknowledgment. This research is supported financially by NSERC (Canada), the Canada Research

Chair program, and the Japan Society for Promotion of Science Fellows (given to R.T.). The Advanced Light Source is supported by the Director, Office of Energy Research, Office of Basic Energy Sciences, Materials Sciences Division of the U.S. Department of Energy, under Contract No. DE-AC03-76SF00098. We thank David Kilcoyne and Tolek Tyliczszak for their expert maintenance and development of the BL 532 facility, Marcia West for excellent work in ultracryomicrotomy, and Mr. Naohiko Saito for his good advice and help. We acknowledge useful contributions from the reviewers, in particular pointing out the possibility of distortion of the analysis by the finite spatial resolution.

References and Notes

- (1) Morgan, L. W. *J. Appl. Polym. Sci.* **1982**, *27*, 2033.
- (2) Okubo, M.; Katsuta, Y.; Matsumoto, T. *J. Polym. Sci., Polym. Lett. Ed.* **1982**, *20*.
- (3) Cho, I.; Lee, K.-W. *J. Appl. Polym. Sci.* **1985**, *30*, 1903.
- (4) Minami, H.; Wang, Z.; Yamashita, T.; Ise, E.; Okubo, M. *Colloid Polym. Sci.* **2003**, *281*, 246.
- (5) Okubo, M.; Takekoh, R.; Suzuki, A. *Colloid Polym. Sci.* **2002**, *280*, 1057.
- (6) Okubo, M.; Izumi, J.; Takekoh, R. *Colloid Polym. Sci.* **1999**, *277*, 875.
- (7) Okubo, M.; Takekoh, R.; Izumi, J. *Colloid Polym. Sci.* **2001**, *279*, 513.
- (8) Okubo, M.; Takekoh, R.; Izumi, J. *Colloid Polym. Sci.* **2003**, *281*, 945.
- (9) Ade, H. In *Experimental Methods In the Physical Sciences*; Samson, J. A. R., Ederer, D. L.; Eds.; Academic Press: San Diego, CA, 1998; Vol 32, p 225.
- (10) Ade, H.; Urquhart, S. G. In *Chemical Applications of Synchrotron Radiation*; Sham, T. K., Ed.; World Scientific Publishing: Singapore, 2002; p 285.
- (11) Kilcoyne, A. L. D.; Tyliczszak, T.; Steele, R.; Hitchcock, P.; Fakra, S.; Frank, K.; Zimba, C.; Rightor, E.; Mitchell, G.; Koprinarov, I.; Anderson, E.; Harteneck, B.; Hitchcock, A. P.; Warwick, T.; Ade, H. *J. Synchrotron Radiat.* **2003**, *10*, 125.
- (12) Stöhr, J. *NEXAFS Spectroscopy*; Springer Tracts in Surface Science; Springer: Berlin, 1992; p 25.
- (13) Rightor, E. G.; Hitchcock, A. P.; Ade, H.; Leapman, R. D.; Urquhart, S. G.; Smith, A. P.; Mitchell, G.; Fischer, D.; Shin, H. J.; Warwick, T. *J. Phys. Chem. B* **1997**, *101*, 1950.
- (14) Koprinarov, I. N.; Hitchcock, A. P.; Li, W. H.; Heng, Y. M.; Stöver, H. D. H. *Macromolecules* **2001**, *34*, 4424.
- (15) Zheng, G.; Croll, L. M.; Hitchcock, A. P.; Stöver, H. D. H. Manuscript in preparation.
- (16) Warwick, T.; Ade, H.; Kilcoyne, A. L. D.; Kritscher, M.; Tyliczszak, T.; Fakra, S.; Hitchcock, A. P.; Hitchcock, P.; Padmore, H. A. *J. Synchrotron Radiat.* **2002**, *9*, 25.
- (17) Jacobsen, C.; Wirick, S.; Flynn, G.; Zimba, C. *J. Microsc.* **2000**, *197*, 173.
- (18) aXis2000, a program optimized for analysis of X-ray images and spectra, is written in Interactive Data Language, and is available from <http://unicorn.mcmaster.ca/aXis2000.html>.
- (19) Koprinarov, I. N.; Hitchcock, A. P.; McCrory, C.; Childs, R. F. *J. Phys. Chem. B* **2002**, *106*, 5358.
- (20) Coffey, T.; Urquhart, S. G.; Ade, H. *J. Electron Spectrosc. Relat. Phenom.* **2002**, *122*, 65.
- (21) Morin, C.; Hitchcock, A. P.; Li, L.; Zhang, X.; Araki, T.; Doran, A.; Scholl, A. *J. Electron Spectrosc. Relat. Phenom.* **2004**, to be submitted.
- (22) Morin, C.; Ikeura-Sekiguchi, H.; Tyliczszak, T.; Cornelius, R.; Brash, J. L.; Hitchcock, A. P.; Scholl, A.; Nolting, F.; Appel, G.; Winesett, A. D.; Kaznatcheyev, K.; Ade, H. *J. Electron Spectrosc.* **2001**, *121*, 203.

MA048609Y